Carbohydrate Research 344 (2009) 204–209

Contents lists available at ScienceDirect

Carbohydrate Research

journal homepage: www.elsevier.com/locate/carres

MALDI-TOF mass spectrometry of naturally occurring mixtures of monorhamnolipids and dirhamnolipids ☆

Neil P. J. Price [a,*], Karen J. Ray [b], Karl Vermillion [c], Tsung-Min Kuo [b]

[a] Bioproducts and Biocatalysis, USDA-ARS-NCAUR, 1815 North University Street, Peoria, IL 61604, USA
[b] Microbial Genomics, USDA-ARS-NCAUR, 1815 North University Street, Peoria, IL 61604, USA
[c] Bioprocessing and New Crops Technology Research Units, USDA-ARS-NCAUR, 1815 North University Street, Peoria, IL 61604, USA

ARTICLE INFO

Article history:
Received 19 August 2008
Received in revised form 10 October 2008
Accepted 15 October 2008
Available online 22 October 2008

We dedicate this paper to the memory of our friend and colleague Tsung-Min Kuo, who passed away on June 10, 2008

Keywords:
Rhamnolipids
Biosurfactants
Mass spectrometry
MALDI-TOFMS
Deuterium-exchange

ABSTRACT

MALDI-TOFMS approaches have been developed for high-throughput screening of naturally occurring mixtures of rhamnolipids from *Pseudomonas* spp. Monorhamnolipids and dirhamnolipids are readily distinguished by characteristic molecular adduct ions, $[M+Na]^+$ and $[M-H+Na_2]^+$, with variously acylated rhamnolipids differing by 28 mu. Following proton-deuterium exchange, deuterated $[M+Na-4^1H+4^2H]^+$ and $[M+Na-6^1H+6^2H]^+$ ions are observed for the monorhamnolipids and dirhamnolipids, respectively, which allows rapid identification of these molecules. The described approach has been validated by compositional analysis using GC/MS, fractionation by RPHPLC, and analysis by 1D and 2D NMR spectroscopy. MALDI-TOFMS analysis allows the rapid screening of variously acylated rhamnolipids, and has potential for selective identification of new surfactants from microbial strains.

Published by Elsevier Ltd.

1. Introduction

Microbial surfactants, which include lipopeptides and glycolipids, are finding increasing application in cosmetics, detergents, as anti-microbials agents, and for oil and mineral recovery.[1–3] Included in the group of glycolipid surfactants are sophorolipids from various yeast species,[4,5] rubiwettins (rubiwettin RG1, β-D-glucopyranosyl-3-[3′-hydroxy-tetradecanoyloxy]-decanoate) from *Serratia rubidaea*,[6] and rhamnolipids from *Pseudomonas* species.[7,8] *Pseudomonas aeruginosa* produces various extracellular α-L-rhamnopyranosyl-β-hydroxyalkanoyl-β-hydroxyalkanoates (monorhamnolipids) and α-L-rhamnopyranosyl-2^1-*O*-α-L-rhamnopyranosyl-β-hydroxyalkanoyl-β-hydroxyalkanoate (dirhamnolipids) composed of L-rhamnose and 3-hydroxyalkanoic acid. Pseudomonads typically produce mixtures of mono- and dirhamnolipids that vary in the acyl moieties (Chart 1), although there are several reports where only monorhamnolipids were detected.[9–11] The O-glycosidically linked aglycone group is always 3-hydroxydecanoate, to

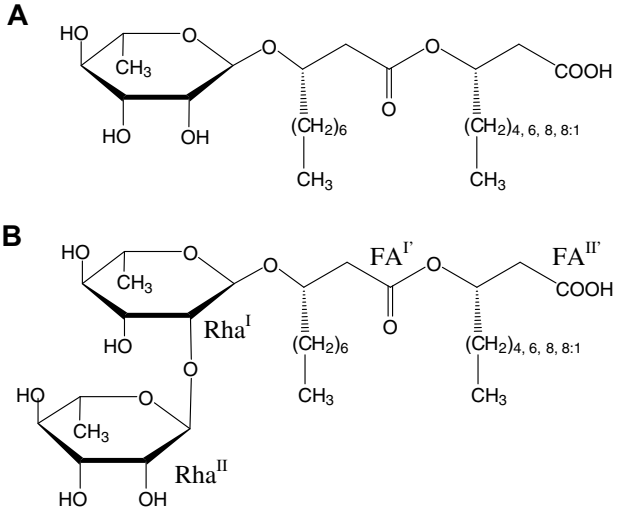

Chart 1. Structures of mono- and dirhamnolipids. (**A**) Monorhamnolipids, Rha-C_{10}-C_8, Rha-C_{10}-C_{10}, Rha-C_{10}-C_{12}; and (**B**) dirhamnolipids, Rha-Rha-C_{10}-C_8, Rha-Rha-C_{10}-C_{10}, Rha-Rha-C_{10}-C_{12}. Rhamnolipids Rha-C_{10}-$C_{12:1}$ and Rha-Rha-C_{10}-$C_{12:1}$ containing unsaturated 3-hydroxyacyl fatty acids were also observed. Nomenclature follows that previously described.[12]

☆ Mention of trade names or commercial products in this article is solely for the purpose of providing specific information and does not imply recommendation or endorsement by the U.S. Department of Agriculture.

* Corresponding author. Tel.: +1 309 681 6246; fax: 1 309 681 6040.
E-mail address: neil.price@ars.usda.gov (N. P. J. Price).

0008-6215/$ - see front matter Published by Elsevier Ltd.
doi:10.1016/j.carres.2008.10.013

which other 3-hydroxyacyl groups may be attached via an ester linkage (Chart 1).

The rhamnolipids have low minimum surface tension (25–32 mN m^{-1}), and low critical micelle concentration (CMC, 5–65 mg L^{-1}).[9] Monorhamnolipids typically have lower CMC values than the corresponding dirhamnolipids. Thus, the CMC for dirhamnolipid α-L-Rha*p*-2^{I}-*O*-α-L-Rha*p*-β-hydroxydecanoyl-β-hydroxydecanoate (Rha-Rha-C_{10}-C_{10}) is 40–65 mg L^{-1}, and for the equivalent monorhamnolipid α-L-Rha*p*-β-hydroxydecanoyl-β-hydroxydecanoate (Rha-C_{10}-C_{10}) is as low as 5 mg L^{-1}.[11] CMC values are more profoundly dependent upon the acyl chain lengths, and the composition of rhamnolipid mixtures therefore influences the ability to solubilize hydrophobic contaminants.[11] The capacity to rapidly analyze rhamnolipid diversity in natural samples is therefore important when screening novel bacterial isolates or for optimizing surface activity.

In this paper, MALDI-TOFMS has been developed as a novel and convenient technique for rapid high-throughput screening of rhamnolipid-containing samples and rhamnolipid-producing *Pseudomonas* sp. The standard multiple-position targets (49 or 100 positions) supplied by Bruker Daltonics allowed about 50 samples to be analyzed in approximately 2.5 h. The facile expedient of proton-deuterium exchange (HX) MALDI-TOFMS allows monorhamnolipids-derived ions to be readily distinguished from those due to dirhamnolipids. MALDI-TOFMS assignments have been verified by GC/MS, HPLC, and NMR spectroscopy, thereby confirming the validity of the method.

2. Results and discussion

2.1. MALDI-TOFMS and deuterium-exchange MALDI-TOFMS analysis

MALDI-TOFMS was used to analyze solvent-extracted rhamnolipids from bacterial cultures and rhamnolipid-producing bacterial colonies from agar plates. The spectra were characterized by molecular ions for monorhamnolipids in the mass range 490–560 mass units, and dirhamnolipids from 640 to 730 mass units (Fig. 1). Major ions at *m/z* 499.4 and *m/z* 527.4 are attributed to the $[M+Na]^+$ adduct ions for the two major monorhamnolipids, α-L-Rha*p*-β-hydroxydecanoyl-β-hydroxyoctanoate (Rha-C_{10}-C_8) and α-L-Rha*p*-β-hydroxy-decanoyl-β-hydroxydecanoate (Rha-C_{10}-C_{10}), respectively (Table 1). The observed 28 mass unit difference corresponds to the mass difference between the C_8 and C_{10} acyl motif. Corresponding $[M-H+Na_2]^+$ disodium adduct ions were observed at *m/z* 521.4 and 549.4. More minor $[M+Na]^+$ molecular ions at *m/z* 555.4 and 553.4 are assigned as Rha-C_{10}-C_{12} and Rha-C_{10}-$C_{12:1}$, respectively (Fig. 1, Table 1). The corresponding dirhamnolipids, α-L-rhamnopyranosyl-2^{I}-*O*-α-L-rhamnopyranosyl-β-hydroxydecanoyl-β-hydroxyoctanoate (Rha-Rha-C_{10}-C_8), β-hydroxyde-canoate (Rha-Rha-C_{10}-C_{10}), -β-hydroxydodecanoate (Rha-Rha-C_{10}-C_{12}), and -β-hydroxydodecenoate (Rha-Rha-C_{10}-$C_{12:1}$), were observed 146 mass units higher, this mass difference being due to the additional rhamnosyl residue. Hence, $[M+Na]^+$ ions are observed for these structures at *m/z* 645.5, 673.5, 701.6, and 699.6, respectively, and the corresponding $[M-H+Na_2]^+$ ions at *m/z* 667.5, 695.6, 723.6, and 721.6 (Fig. 1). These molecular adducts ions were also observed after the separation of rhamnolipid fractions by reverse-phase HPLC and analysis by MALDI-TOFMS (Table S1). As this is generally the case with MALDI-TOFMS analysis of glycolipids, occasional $[M+K]^+$ potassium adduct ions were also observed (Table 1).

Additional $[M+Na+14]^+$ ions due to rhamnolipid methyl esters were seen when the MALDI-TOFMS 2,5-DHB matrix and samples were dissolved in methanol (Fig. S1). Hence, ions at *m/z* 513.4 and 541.5 are due to methyl esters of monorhamnolipids Rha-C_{10}-C_8 and Rha-C_{10}-C_{10}. Similarly, $[M+Na+14]^+$ ions at *m/z* 659.5 and 687.5 are due to the methyl esters of the Rha-Rha-C_{10}-C_8, Rha-Rha-C_{10}-C_{10}, and Rha-Rha-C_{10}-C_{12} dirhamnolipids (Fig. S1). The methyl ester ions were not seen when the 2,5-DHB matrix was dissolved in either ethyl acetate (data not shown) or acetonitrile (Fig. S1).

Deuterium-exchange MALDI-TOF mass spectrometry (HX MALDI-TOFMS) was used to confirm the identity of the

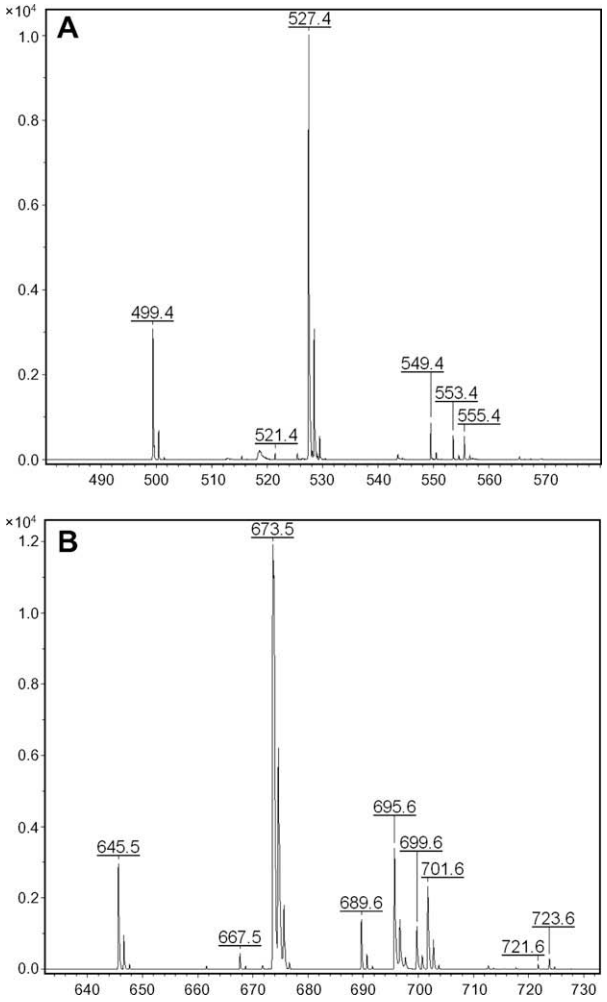

Figure 1. MALDI-TOFMS $[M+Na]^+$ and $[M-H+Na_2]^+$ molecular ions of (**A**) monorhamnolipids, and (**B**) dirhamnolipids. Assignments are listed in Table 1.

Table 1
Rhamnolipids molecular ions observed by MALDI-TOFMS

Acyl group	Molecular formula	$[M+Na]^+$		$[M+K]^+$		$[M-H+Na_2]^+$	
		Obsd	[a]Calcd	Obsd	Calcd	Obsd	Calcd
Monorhamnolipids							
C_{10}–C_8	$C_{24}H_{44}O_9$	499.401	499.288	—	515.262	521.378	521.270
C_{10}–C_{10}	$C_{26}H_{48}O_9$	527.377	527.320	—	543.293	549.380	549.302
C_{10}–C_{12}	$C_{28}H_{52}O_9$	555.442	555.351	—	571.325	—	577.333
C_{10}–$C_{12:1}$	$C_{28}H_{50}O_9$	553.434	553.335	—	569.309	—	575.317
Dirhamnolipids							
C_{10}–C_8	$C_{30}H_{54}O_{13}$	645.516	645.346	661.508	661.320	667.550	667.328
C_{10}–C_{10}	$C_{32}H_{58}O_{13}$	673.517	673.378	689.564	689.351	695.584	695.359
C_{10}–C_{12}	$C_{34}H_{62}O_{13}$	701.628	701.409	—	717.383	723.643	723.391
C_{10}–$C_{12:1}$	$C_{34}H_{60}O_{13}$	699.611	699.393	—	715.367	721.640	721.375

[a] Monoisotopic masses were calculated using ISOPRO 3.0.

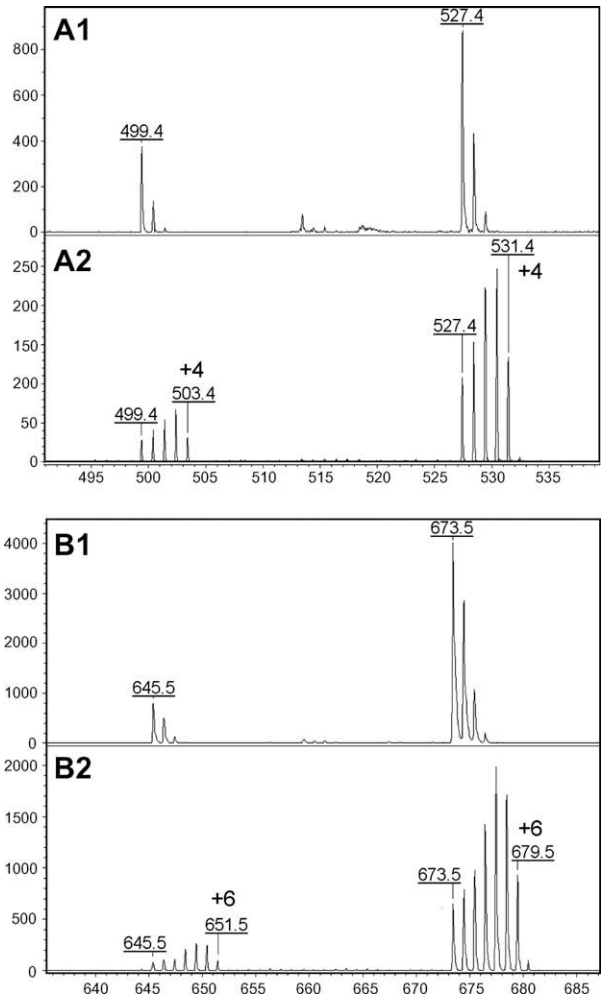

Figure 2. Deuterium-exchanged $[M+Na+4]^+$ MALDI-TOFMS ions for monorhamnolipids (panel A2) and $[M+Na+6]^+$ ions for dirhamnolipids (panel B2). Corresponding non-exchanged controls are shown in panels A1 and B1, respectively.

rhamnolipid-derived ions. This required the exchange of labile hydroxyl protons for deuterium atoms, with an expected corresponding increase in mass due to the number of exchanges.[22] Hence, monorhamnolipids were expected to undergo 4 exchanges (3 rhamnosyl hydroxyl groups plus 1 carboxylate) and dirhamnolipids to undergo 6 exchanges (5 rhamnosyl hydroxyls plus 1 carboxylate). Following deuterium exchange, the major monorhamnolipids Rha-C_{10}-C_8 and Rha-C_{10}-C_{10} were observed as series of $[M+Na]^+$ ions clusters up to $[M+Na+4]^+$ (Fig. 2). The corresponding dirhamnolipids, Rha-Rha-C_{10}-C_8 and Rha-Rha-C_{10}-C_{10}, were evident as $[M+Na+6]^+$ ion clusters, evidence of the 6 exchangeable groups present on the dirhamnolipid species (Fig. 2). Hence, this provides a straightforward and rapid way of confirming the mass assignments. Exchanged $[M+Na+6]^+$ ions were also observed for the minor dirhamnolipids Rha-Rha-C_{10}-C_{12} and Rha-Rha-C_{10}-$C_{12:1}$ (data not shown), although for these assignments were complicated by overlap of the respective exchanged ion clusters.

2.2. Lipid and sugar compositional analysis by GC/MS

To confirm the MALDI-TOFMS assignments and provide additional structural data, the rhamnolipid extracts were analyzed by GC/MS for composition and by NMR spectroscopy. Acid-hydrolyzed or saponified samples were derivatized to form volatile aldononitrile peracetates (PAANs) and fatty acid methyl esters (FAMES) suitable for GC/MS analysis of sugars and lipids. For the lipids, GC peaks were observed for hydroxydecanoate, hydroxyoctanoate, and hydroxydodecanoate, although the expected minor unsaturated hydroxydodecenoate was below the detection limit. The FAMES mass spectra contained major *m/z* 103 fragment ions (Fig. 3, Panel A) that are characteristic of 3-hydroxy fatty acids.[23] For the sugar derivatives, a single GC peak was observed that co-eluted with a standard of L-rhamnose PAAN. The MS spectra arising from this peak showed *m/z* 117 and 129 fragment ions that are characteristic of 6-deoxyhexoses (Fig. 3, Panel B) and identical to the standard L-rhamnose PAAN.[24] These data were consistent with the MALDI-TOFMS analysis and the subsequent NMR data.

2.3. 1D and 2D NMR assignments

^1H and ^{13}C NMR spectra and correlation spectra (COSY, HSQC, and HMBC) were obtained on rhamnolipid-containing samples (Figs. 4 and 5, Fig. S2, Table 2). Two major α-L-rhamnosyl anomeric protons, Rha^I H-1^I and Rha^{II} H-1^{II}, were apparent as overlapping doublets at 4.94 and 4.92 ppm, respectively. In the HSQC spectrum, these are seen to correlate to anomeric carbon signals at 98.0 and 103.0 ppm, respectively (Fig. 5). Less intense anomeric proton and carbon signals at 4.91 and 99.5 ppm are attributed to the small amount of monorhamnolipids present (Fig. 5). COSY correlations are seen from the major anomeric proton signals to the two rhamnosyl H-2 protons at 3.72 and 3.98 ppm (Fig. 4). The signal at 3.72 ppm is assigned to Rha^I, adjacent to the lipid motif, while 3.98 ppm is from H-2^{II} of Rha^{II}. In the HSQC spectrum, these show correlations to ^{13}C nuclei at 79.2 and 70.5 ppm, respectively (Fig. 5). The former shift (79.2 ppm) is indicative of the glycosidic substitution at O-2^I on this residue. The rhamnosyl methyl protons are assigned to the two overlapping doublets at 1.25 ppm, and show strong COSY correlations to H-5^I and H-5^{II} proton signals at 3.65 ppm. The rhamnosyl methyl ^{13}C signals at 16.5 ppm are assigned from the HSQC spectrum (Fig. 5). Long-range HMBC couplings are observed from these methyl ^{13}C signals to protons in the 3.5–4.0 ppm region, assigned as rhamnosyl ring protons (Fig. S2).

The 3-hydroxyacyl lipid motifs are evident from the two 3-hydroxymethine protons, H-$3^{II'}$ at 5.27 and H-$3^{I'}$ at 4.08 ppm (Fig. 5). HSQC and COSY spectra indicate that the former is coupled to C-$3^{II'}$ at 71.0 ppm, and to two methylene protons at 2.59 and 1.63 ppm (Figs. 4 and 5). Similarly, the $FA^{I'}$ H-$3^{I'}$ methine proton at 4.08 ppm is coupled to C-$3^{I'}$ at 74.0 ppm, and protons H-$2^{I'}$ and H-$4^{I'}$ at 2.50 and 1.58 ppm, respectively. The two H-4 methylenes (1.63 and 1.58 ppm) are also coupled to the $-CH_2-$ chain protons observed at 1.4 ppm, and hence to the acyl methyl protons at 0.90 ppm. The corresponding methyl carbons (13.0 ppm), C-$2^{I'}$ and C-$2^{II'}$ carbons (40.0 and 38.5 ppm), and C-$4^{I'}$ and C-$4^{II'}$ carbons (33.0 and 33.8 ppm) are assigned from the HSQC spectrum (Fig. 5).

Confirmations for several of these assignments are evident from long-range HMBC couplings (Fig. S2, Table 2). Two FA carboxyl groups, C-$1^{I'}$ (ester) and C-$1^{II'}$ (free acid) are evident at 171.1 and 173.0 ppm, respectively. The free acid C-$1^{II'}$ is coupled to the adjacent H-$2^{II'}$ methylene (2.59 ppm) and to the H-$3^{II'}$ hydroxymethine (5.27 ppm). The FA ester C-$1^{I'}$ is similarly coupled to H-$2^{I'}$ and H-$3^{I'}$ (2.50 and 4.08 ppm, respectively), but shows an additional coupling across the ester bridge oxygen to H-$3^{II'}$ (5.27 ppm). The Rha^I anomeric carbon C-1^I (98.0 ppm) shows 3-bond coupling across the O-glycosidic bond to the $FA^{I'}$ H-$3^{I'}$ hydroxymethine proton (4.08 ppm) confirming that this rhamnosyl residue is O-glycosidically linked to the $FA^{I'}$ acyl motif. Similarly, the Rha^{II} anomeric carbon (C-1^{II}, 103.0 ppm) is coupled across the 2^I-O-glycosidic bridge oxygen to the Rha^I H-2^I proton (3.72 ppm) (Supplementary Fig. S2). These latter data confirm the alpha-L-Rha-(1→2) linkage between the two rhamnose residues.

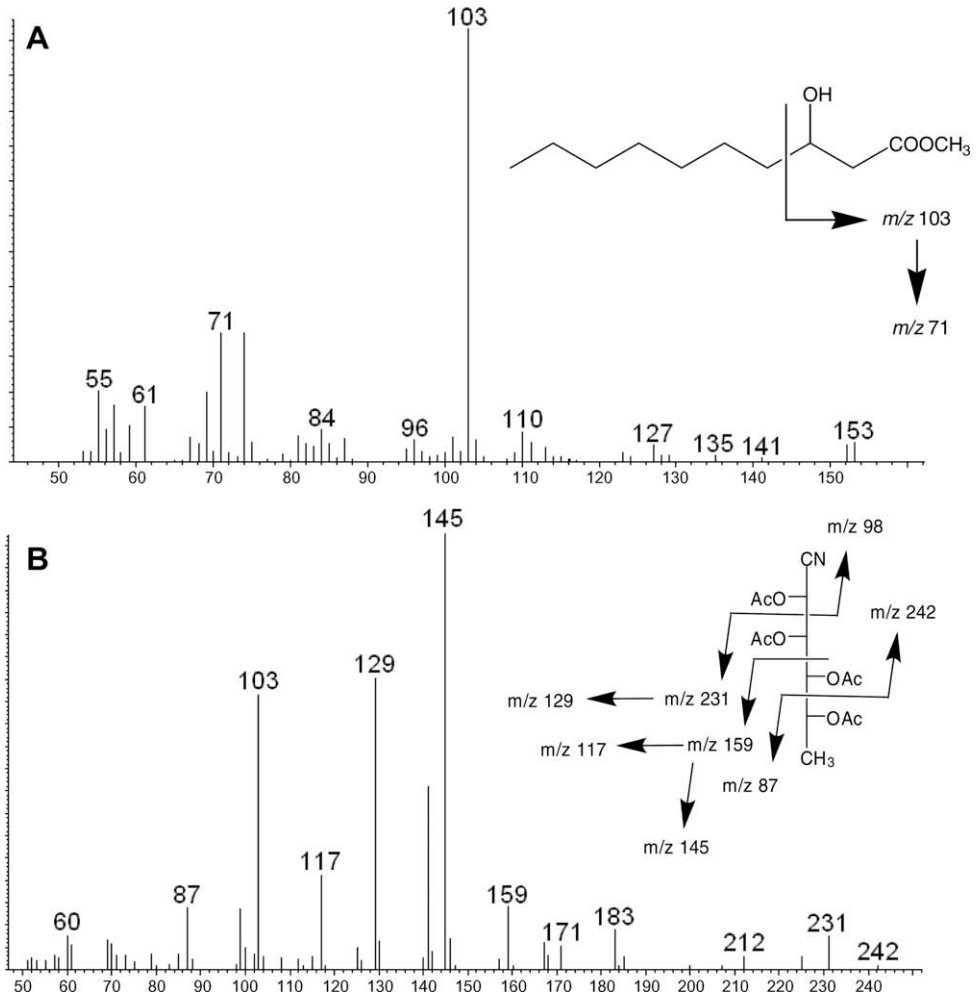

Figure 3. GC/MS spectra and MS ion fragmentation assignments. (**A**) 3-Hydroxydecanoic acid methyl ester; and (**B**) L-rhamnose aldononitrile acetate.

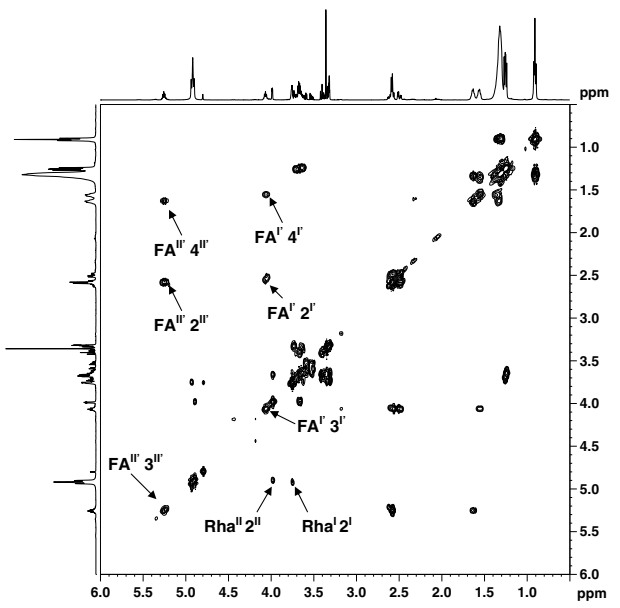

Figure 4. ^{1}H–^{1}H correlation spectrum (COSY). The rhamnosyl Rha^{I} and Rha^{II} $J_{1,2}$ couplings are arrowed. The FA$^{I'}$ and FA$^{II'}$ acyl groups 3$^{I'}$-*CH*-*O*-Rha^{I} and 3$^{II'}$-*CH*-*O*-acyl methine signals, and the *J*-coupled 2$^{I'}$*CH*$_2$, 4$^{I'}$*CH*$_2$, and 2$^{II'}$*CH*$_2$, 4$^{II'}$*CH*$_2$ methylenes are also indicated. The complete NMR assignments are listed in Table 2.

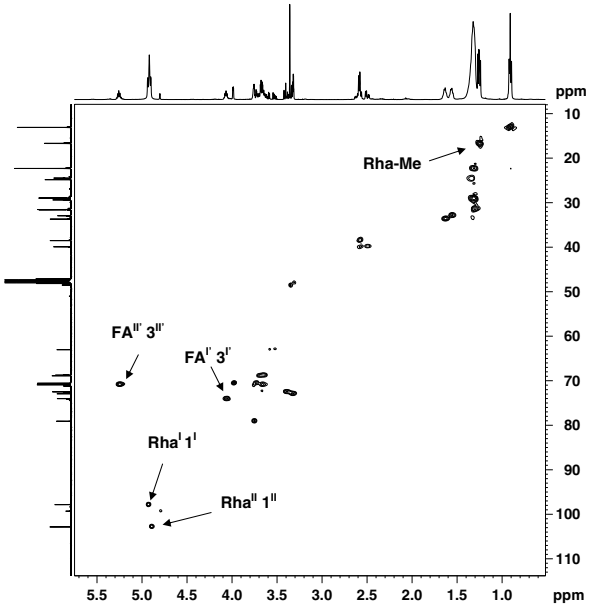

Figure 5. ^{1}H–^{13}C short-range correlation spectrum (HSQC). The rhamnosyl anomeric ^{1}H–^{13}C couplings (Rha^{I} 1^{I} and Rha^{II} 1^{II}), and rhamnosyl position-6 methyl groups (Rha-Me) are arrowed. The acyl groups 3$^{II'}$-*CH*-*O*-acyl (FA$^{II'}$ 3$^{II'}$) and 3$^{I'}$-*CH*-*O*-Rha (FA$^{I'}$ 3$^{I'}$) ^{1}H–^{13}C correlations are also indicated. Other assignments are listed in Table 2.

Table 2
^{1}H and ^{13}C NMR data and assignments

Residue	Chemical shifts[a] (ppm) and assignments			
	Proton	δ_H	Carbon	δ_C
L-Rha^{I}				
	H-1^{I} anomeric	4.94	C-1^{I}	98.0
	H-2^{I}	3.72	C-2^{I}	79.2
	H-3^{I}	—	C-3^{I}	—
	H-4^{I}	—	C-4^{I}	—
	H-5^{I}	3.65	C-5^{I}	—
	H-6^{I} methyl	1.25	C-6^{I} methyl	16.5
L-Rha^{II}				
	H-1^{II} anomeric	4.92	C-1^{II}	103.0
	H-2^{II}	3.98	C-2^{II}	70.5
	H-3^{II}	—	C-3^{II}	—
	H-4^{II}	—	C-4^{II}	—
	H-5^{II}	3.65	C-5^{II}	—
	H-6^{II} methyl	1.25	C-6^{II} methyl	16.5
3-Hydroxyacyl FA$^{I'}$				
			C-1$^{I'}$ (ester)	171.1
	H-2$^{I'}$	2.50	C-2$^{I'}$	40.0
	H-3$^{I'}$	4.08	C-3$^{I'}$	74.0
	H-4$^{I'}$	1.58	C-4$^{I'}$	33.0
	–C*H*$_2$– chain	1.4	–C*H*$_2$– chain	29–30
	C*H*$_3$–	0.90	C*H*$_3$–	13.0
3-Hydroxyacyl FA$^{II'}$				
			C-1$^{II'}$(acid)	173.0
	H-2$^{II'}$	2.59	C-2$^{II'}$	38.5
	H-3$^{II'}$	5.27	C-3$^{II'}$	71.0
	H-4$^{II'}$	1.63	C-4$^{II'}$	33.8
	–C*H*$_2$– chain	1.4	–C*H*$_2$– chain	29–30
	C*H*$_3$–	0.90	C*H*$_3$–	13.0

[a] Samples were dissolved in MeOH-d_4.

2.4. Conclusions

To date, screening for rhamnolipids has relied on colorimetric detection of the rhamnose groups. However, this provides minimal structural information, and is susceptible to interference by other sugars. Structural characterization of rhamnolipids has relied on electrospray ionization mass spectrometry, coupled with either on- or off-line column chromatography,[12–16] fast atom bombardment mass spectrometry (FABMS),[17,18] NMR spectroscopy,[12,19] and compositional monosaccharide and lipid analysis by gas chromatography-mass spectrometry.[12–14] FABMS analysis has also been coupled with high-performance thin layer chromatography.[20] In one case, derivatized rhamnolipid bromophenacyl esters have been analyzed by reversed-phase HPLC in order to improve chromatographic resolution.[9] These techniques are well suited for structural analysis, but are less suitable for high-throughput screening of relatively crude bacterial extracts. Here, we describe the novel application of MALDI-TOFMS and deuterium-exchange HX-MALDI-TOFMS for the rapid analysis of mono- and dirhamnolipids. The approach is validated by carbohydrate and lipid GC/MS analysis, RPHPLC, and 1D and 2D NMR. The rapid, MS-based techniques presently described allow for sensitive and specific screening of variously acylated rhamnolipids in bacterial extracts, and have potential for rapidly identifying new biosurfactant-producing strains.

3. Experimental

3.1. Bacterial fermentation and extraction

Bacterial cultures from soil samples collected at West Central Cooperative, Ralston, IA were grown in modified Kay's medium[21] containing glycerol (0.5% v/v), and transferred to production medium containing glycerol (10 g L^{-1}), ammonium sulfate (1 g L^{-1}), disodium phosphate (3.53 g L^{-1}), potassium dihydrogen phosphate (3.40 g L^{-1}), citric acid (0.4 g L^{-1}), $MgSO_4{\cdot}7H_2O$ (0.40 g L^{-1}), and $CaCl_2{\cdot}2H_2O$ (0.4 g L^{-1}), plus trace metal elements (Fe, Mo, and Mn). After growth in shaker flasks (72 h, 30 °C; 250 rpm) the cultures were extracted twice with equal vols of EtOAc. In some cases, the rhamnolipid-containing extracts were back-washed with hexane.

3.2. Compositional analysis by gas chromatography/mass spectrometry (GC/MS)

Samples were hydrolyzed in dry methanolic HCl (100 mM, 80 °C) on a reaction block. After cooling, the solvent was removed by evaporation and the residue was dissolved in MeCN (typically 200 μL). Aldononitrile acetates were prepared as described previously.[24] GC/MS analysis was performed on an Agilent (Santa Clara, CA) 6890N gas chromatograph interfaced with an Agilent 5973N mass-selective detector configured in EI mode, and with a Hewlett Packard (Santa Clara, CA) 7683 series autoinjector. In GC a Hewlett Packard DB-5ms column (30 m by 0.2 mm) was used with helium as the carrier and a linear gradient from 150 to 300 °C at 10 °C per min. Mass spectra were recorded in positive-ion mode over the range *m/z* 60–550. Injector and detector/interface temperatures were 275 and 300 °C, respectively. Data analysis was done off-line using HP Chemstation.

3.3. Reversed-phase high-performance liquid chromatography (RPHPLC)

The HPLC instrument was a Finnigan Surveyor (Thermo Fisher Scientific, Waltham, MA). RPHPLC was essentially as described,[12] using a Thermo Hypersil GOLD 100 × 4.6 mm C-18 column (5 μm particle size). The mobile phase was a 20–90% v/v aq MeCN gradient (30 min run time), with a flow rate of 1 mL min^{-1}. Elution was monitored with a diode array detector.

3.4. MALDI-TOFMS and proton-exchange (HX) MALDI-TOFMS analysis

MALDI-TOF mass spectra were recorded on a Bruker Daltonic Omniflex instrument (Bruker Daltonics, Billerica, MA) operating in reflectron mode. Samples were typically dissolved in MeCN, and the matrix used was 2,5-dihydrobenzoic acid. Deuterium-exchange was obtained by dissolving the samples and matrix in 4:1 MeOH-d_4 (98.8% D)–D_2O (99.96% D). The exchanged samples plus matrix were dried onto the target at room temperature prior to introduction into the spectrometer. Ion source 1 was set to 19.0 kV, and source 2 to 14.0 kV, with lens and reflector voltages of 9.20 and 20.00 kV, respectively. A 200 ns pulsed ion extraction was used with matrix suppression up to 200 Da. The instrument was calibrated externally on a dp series of malto-oligosaccharides. Excitation was at 337.1 nm, typically at 60% of 150 μJ maximum output, and 80 shots were accumulated. The linear mass resolution (FWHM) for *m/z* 2465 (ACTH 18-39) was >3500.

3.5. NMR spectroscopy

All NMR experiments were performed on a Bruker Avance spectrometer (Bruker BioSpin Corp., Billerica, MA) operating at 500.11 MHz using a standard 5 mm *z*-gradient BBI probe at 27 °C. Chemical shifts are reported as ppm from tetramethylsilane calculated from the lock solvent. The deuterated solvents used were obtained from Cambridge Isotope Labs (Andover, MA). The pulse sequences used were those supplied by Bruker, and processing was done with the Bruker TOPSPIN software package (version 1.3).

Acknowledgments

We acknowledge the technical assistance of Trina Hartman, and helpful discussion and pre-review of the manuscript by Karen Hughes and Dr. Joseph Rich (NCAUR-ARS-USDA, Peoria).

Supplementary data

Supplementary data associated with this article can be found, in the online version, at doi:10.1016/j.carres.2008.10.013.

References

1. Georgiou, G.; Lin, S.-C.; Sharma, M. M. *Biotechnology* **1992**, *10*, 60–65.
2. Cooper, D. G.; Zajic, J. E. *Adv. Appl. Microbiol.* **1980**, *26*, 229–253.
3. Dembitsky, V. M. *Lipids* **2004**, *39*, 933–953.
4. Van Bogaert, I. N.; Saerens, K.; De Muynck, C.; Develter, D.; Soetaert, W.; Vandamme, E. J. *Appl. Microbiol. Biotechnol.* **2007**, *76*, 23–34.
5. Koster, C. G.; Heerma, W.; Pepermans, H. A.; Groenewegen, A.; Peters, H.; Haverkamp, J. *Anal. Biochem.* **1995**, *230*, 135–148.
6. Matsuyama, T.; Kaneda, K.; Ishizuka, I.; Toida, T.; Yano, I. *J. Bacteriol.* **1990**, *172*, 3015–3022.
7. Maier, R. M.; Soberón-Chávez, G. *Appl. Microbiol. Biotechnol.* **2000**, *54*, 625–633.
8. Lang, S.; Wullbrandt, D. *Appl. Microbiol. Biotechnol.* **1999**, *51*, 22–32.
9. Lebrón-Paler, A.; Pemberton, J. E.; Becker, B. A.; Otto, W. H.; Larive, C. K.; Maier, R. M. *Anal. Chem.* **2006**, *78*, 7649–7658.
10. Gunther, N. W.; Nunez, A.; Fett, W.; Solaiman, D. K. Y. *Appl. Environ. Microbiol.* **2005**, *71*, 2288–2293.
11. Mata-Sandoval, J. C.; Karns, J.; Torrents, A. *J. Chromatogr., A* **1999**, *864*, 211–220.
12. Sharma, A.; Jansen, R.; Nimtz, M.; Johri, B. N.; Wray, V. *J. Nat. Prod.* **2007**, *270*, 941–947.
13. Monteiro, S. A.; Sassaki, G. L.; de Souza, L. M.; Meira, J. A.; de Araújo, J. M.; Mitchell, D. A.; Ramos, L. P.; Krieger, N. *Chem. Phys. Lipids* **2007**, *147*, 1–13.
14. Howe, J.; Bauer, J.; Andrä, J.; Schromm, A. B.; Ernst, M.; Rössle, M.; Zähringer, U.; Rademann, J.; Brandenburg, K. *FEBS J.* **2006**, *273*, 5101–5112.
15. Déziel, E.; Lépine, F.; Milot, S.; Villemur, R. *Biochim. Biophys. Acta* **2000**, *1485*, 145–152.
16. Déziel, E.; Lépine, F.; Dennie, D.; Boismenu, D.; Mamer, O. A.; Villemur, R. *Biochim. Biophys. Acta* **1999**, *1440*, 244–252.
17. Denekamp, C.; Claeys, M.; Pocsfalvi, G. *Rapid Commun. Mass Spectrom.* **2000**, *14*, 794–799.
18. Manso Pajarron, A.; De Koster, G. C.; Heerma, W.; Schmidt, M.; Haverkamp, J. *Glycoconjugate J.* **1993**, *10*, 219–226.
19. Choe, B.-Y.; Krishna, R. N.; Pritchard, D. G. *Magn. Reson. Chem.* **1992**, *30*, 1025–1026.
20. de Koster, G. C.; Vos, B.; Versluis, C.; Heerma, W.; Haverkamp, J. *Biol. Mass Spectrom.* **1994**, *23*, 179–185.
21. Zhang, Y.; Miller, R. M. *Appl. Environ. Microbiol.* **1992**, *58*, 3276–3282.
22. Price, N. P. J. *Anal. Chem.* **2006**, *78*, 5302–5308.
23. Yang, S.-Y.; Wei, D. Z.; Mu, B. Z. *J. Biochem. Biophys. Methods* **2007**, *70*, 519–523.
24. Price, N. P. J. *Anal. Chem.* **2004**, *76*, 6566–6574.